Electronic Supplementary Material (ESI) for ChemComm.

Electronic Supporting Information (ESI) to the article

Structure and dynamics elucidation of ionic liquids by multidimensional Laplace NMR

*Muhammad Asadullah Javed, Susanna Ahola, Pär Håkansson, Otto Mankinen, Muhammad Kamran Aslam, Andrei Filippov, Faiz Ullah Shah, Sergei Glavatskih, Oleg. N. Antzutkin and Ville-Veikko Telkki**

Contents

1. Experimental

1.1 Sample preparation

The ionic liquid (IL) under study consisting of trihexyl(tetradecyl)phosphonium cations, $[P_{6,6,6,14}]^+$, and bis(mandelato)borate anions, $[BMB]^-$, was synthesised in the group of Chemistry of Interfaces at Luleå University of Technology [1]. In the present work, initially a thin layer of the IL was kept under vacuum (pressure less than 10^{-3} mbar) at 383 K for 4 h in order to remove residual moisture. Then 300 µl of the IL was transferred into a 5 mm glass tube and ^{129}Xe gas at 1 atm was added to the tube. After that the tube was sealed with a flame.

1.2 NMR experiments

^{1}H NMR diffusion measurements were carried out as a function of temperature with temperature stabilisation time of 30 minutes using a PGSTE experiment with bipolar gradients. The low temperature experiments (296, 303 and 309 K) were carried out by Bruker Avance III 300 MHz spectrometer at 7 T, using a Diff 50 diffusion probe. The maximum gradient strength was 9.49 Tm^{-1}. The high temperature experiments (above 320 K) were carried out at Avance III 600 MHz spectrometer at 14 T, using a BBFO probe. The maximum gradient strength was 0.48 Tm^{-1}. In all the experiments, the diffusion time Δ was 100 ms, the number of gradient steps was 64 and 8 scans were acquired. In the low temperature experiments, the length of the gradient pulse δ was varied from 4 to 6.7 ms, while in the high temperature experiments the length of the gradient pulse δ was varied from 12 to 30 ms.

In the ***D*-T_2 experiment**, the maximum diffusion gradient strength was 9.49 Tm^{-1}, the number of gradient steps was 16, the lengths of the gradient pulse was 3.5 ms, and the diffusion time Δ was 100 ms. In the CPMG T_2 block, the number of echoes was 32, and the echo time was 2 ms. The experiment was done at 296 K with 32 scans and the total experiment time was approximately 19 hours.

In the T_2-T_2 **exchange experiment**, the number of echoes in both CPMG blocks was 32, and the echo time was 2 ms. The mixing times were 50, 100, 200 and 400 ms. The experiment was carried out at 296 K. The total experiment time with 8 scans was about 8 hours.

2. Experimental results

2.1 ^{1}H NMR spectra

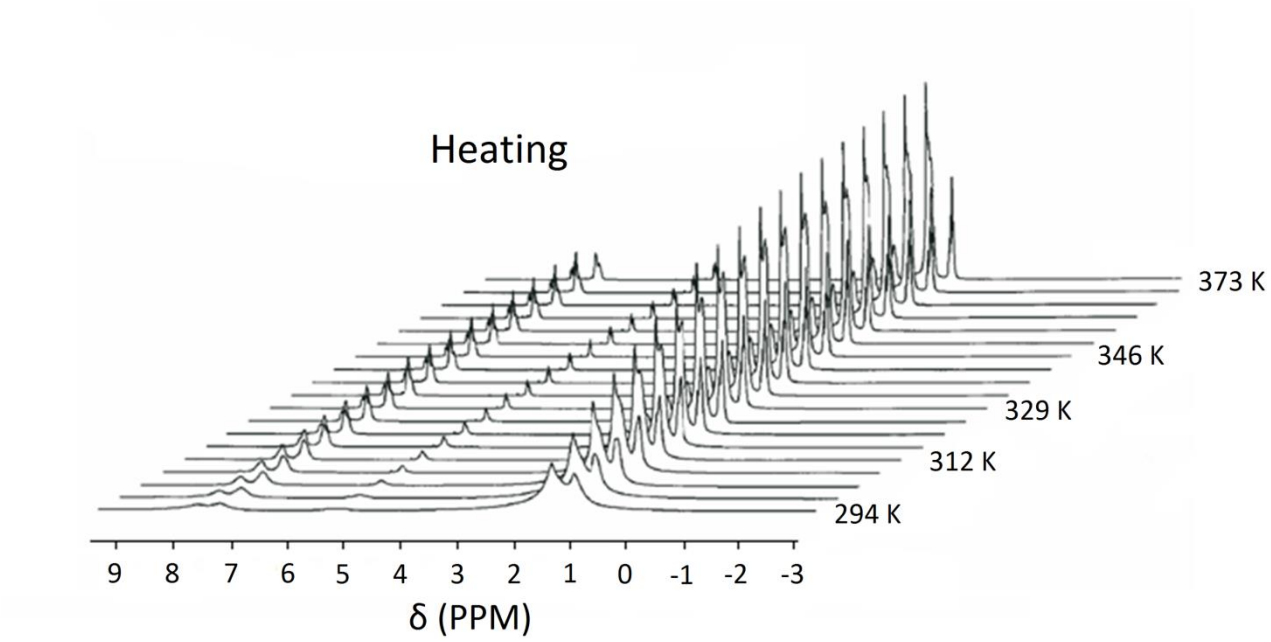

Figure S1. 300 MHz ^{1}H NMR spectra of $[P_{6,6,6,14}][BMB]$ as a function of temperature. The resonance lines become much broader below 320 K due to reduced mobility of ions in the IL. This may be a consequence of either homogeneous or inhomogeneous line broadening.

2.2 1D Diffusion

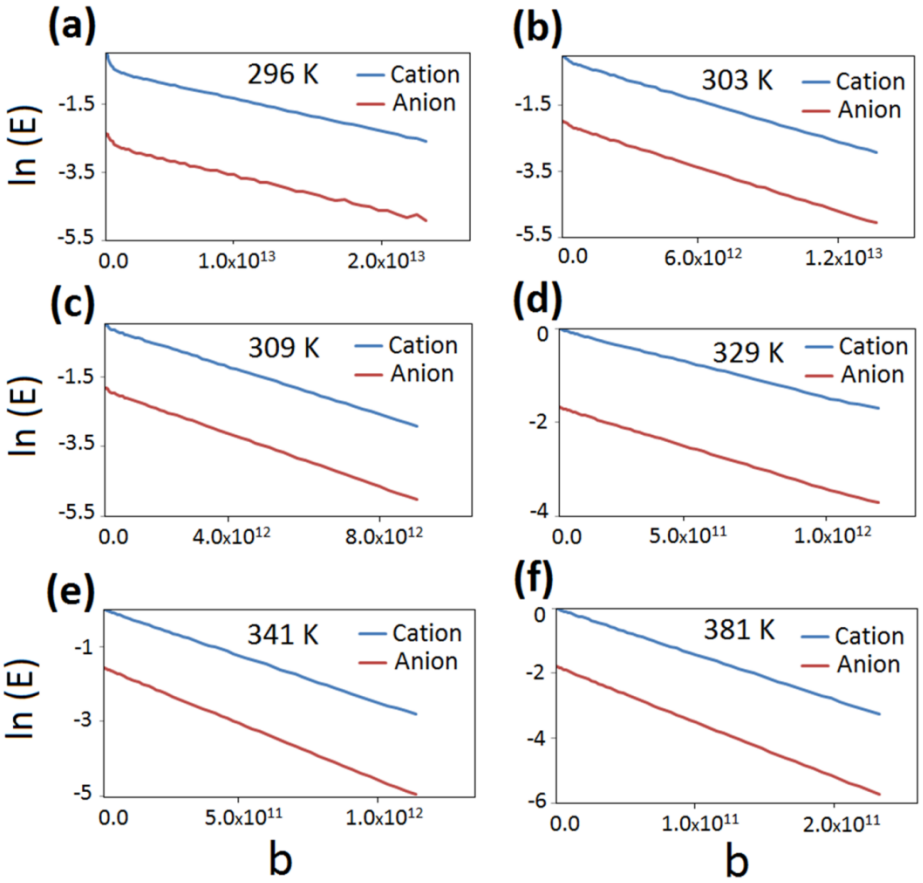

Figure S2. Natural logarithm of the signal amplitude E in the ^{1}H PGSTE-BP diffusion NMR experiments on [$P_{6,6,6,14}$][BMB] as a function of $b=\gamma^2\delta^2g^2(\Delta-\delta/3)$. Here, γ is the gyromagnetic ratio of ^{1}H, δ and g are the amplitude and duration of gradients and Δ is the diffusion time. The dependencies are clearly non-linear at the temperatures between 296 and 309 K, indicating that there are more than two diffusion components. Laplace inversion of the signal amplitudes E resulted in the D distributions shown in Figures 1c and 1d.

The temperature dependence of the diffusion coefficient is represented by the Arrhenius function

$$D = D_0 \exp\left(\frac{-E_D}{RT}\right), \tag{S1}$$

where D_0 is the pre-exponential factor, E_D is the activation energy for diffusion, and R is the gas constant. By taking natural logarithm on both sides, equation (S1) becomes as follows:

$$\ln D = \ln D_0 - \left(\frac{-E_D}{R}\frac{1}{T}\right). \tag{S2}$$

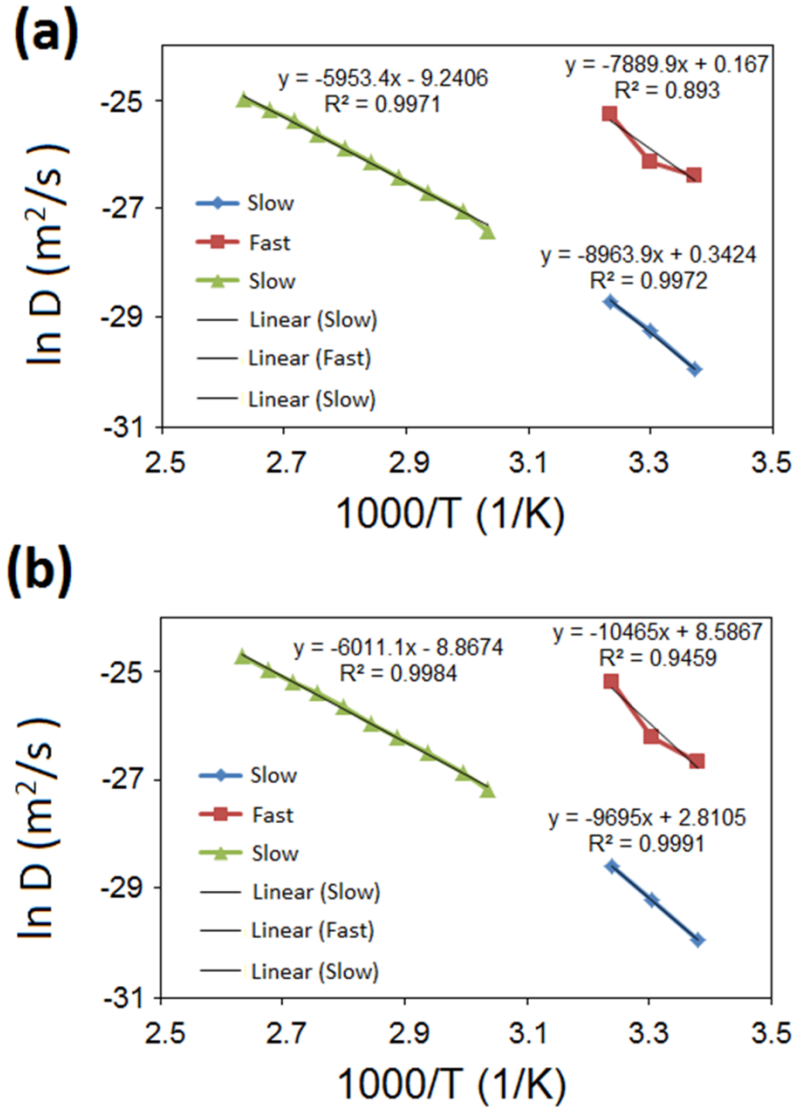

Figure S3. Arrhenius plots for (a) the cation and (b) the anion. For the cation, at low temperatures (high 1000/*T*), the activation energy of the slowly diffusing phase is 75±5 kJ/mol, while for the fast diffusing component it is 70±30 kJ/mol. At higher temperatures, where there is only a single phase, the activation energy is 49.6±1.0 kJ/mol. In case of the anion at low temperatures, the activation energy of the slowly diffusing phase is 81±3 kJ/mol, while for the fast diffusing phase it is 90±30 kJ/mol. At higher temperatures, where there is only a single phase, the activation energy is 50.0±0.8 kJ/mol.

2.3 Relaxation measurements

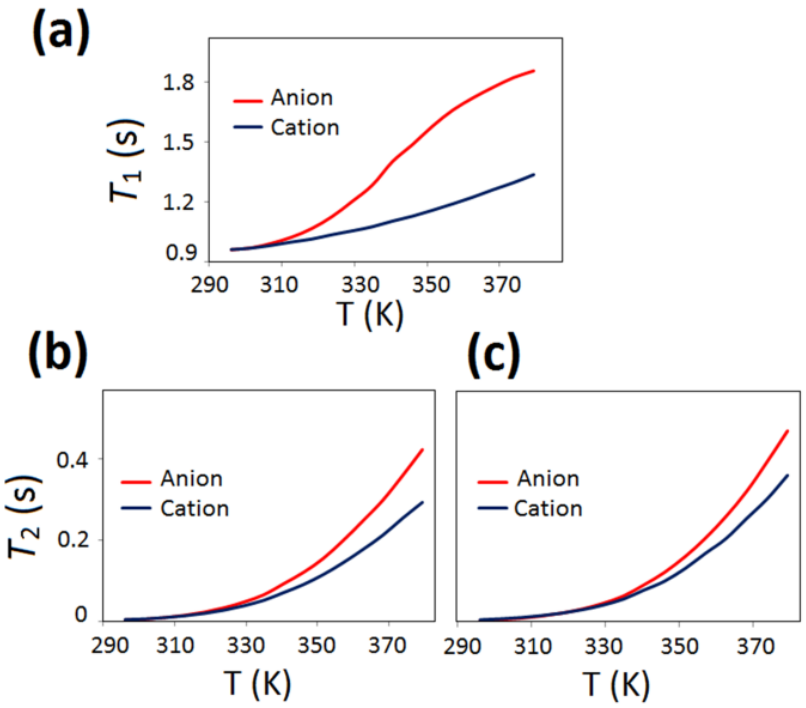

Figure S4. (a) ^{1}H T_1 relaxation times of [$P_{6,6,6,14}$][BMB] IL measured by the inversion recovery pulse sequence for the anion and the cation. Only a single relaxation time component was observed because of exchange averaging. T_2 relaxation times measured by the (b) CPMG and (c) PROJECT [2] experiments as the values were obtained from a single exponential fit to the experimental data. The values reflect the T_2 in the slow phase, which is dominating in the whole temperature range. PROJECT removes the effect of homonuclear *J*-couplings on the amplitude decay. Because the T_2 values measured by the CPMG and PROJECT methods are in quite good agreement, the effect of homonuclear *J*-couplings is insignificant for [$P_{6,6,6,14}$][BMB] IL.

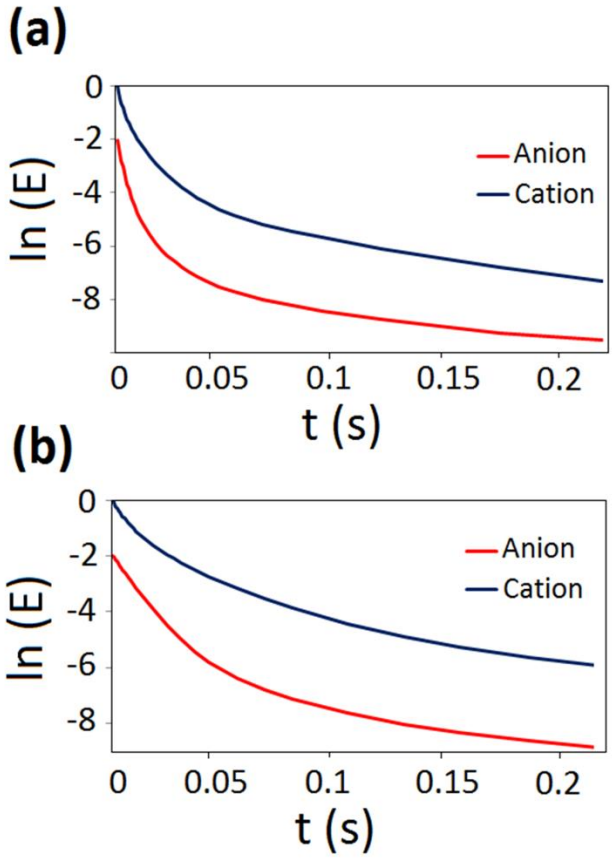

Figure S5. Natural logarithm of the signal amplitude *E* as a function of time *t* in the ^{1}H CPMG NMR experiments carried out at (a) 296 K and (b) 309 K. Nonlinear behaviour shows that there are a few T_2 components. Laplace inversion of the signal amplitude *E* resulted in the T_2 distribution shown in Figure 2b.

2.4 ^{129}Xe NMR spectra

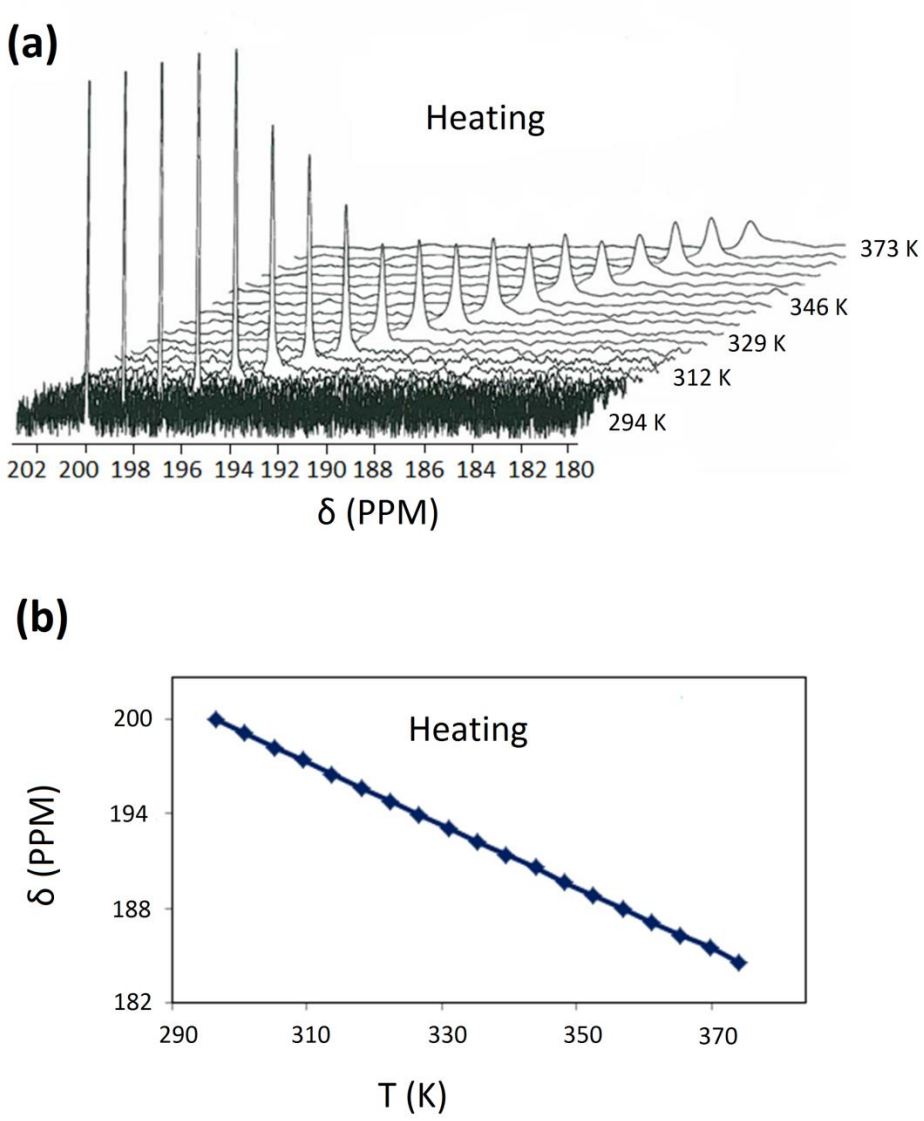

Figure S6. (a) ^{129}Xe NMR spectra of xenon dissolved in [$P_{6,6,6,14}$][BMB] measured at 7.1 T (^{129}Xe frequency 83.0 MHz). Increased linewidth at high temperatures (T > 329 K) reflects increased temperature gradients in the sample. (b) The chemical shift of ^{129}Xe as a function of temperature. Linear behaviour indicates that there are no abrupt changes in the density or orientation of ions in the IL.

2.5 T_2-T_2 relaxation exchange for the anion

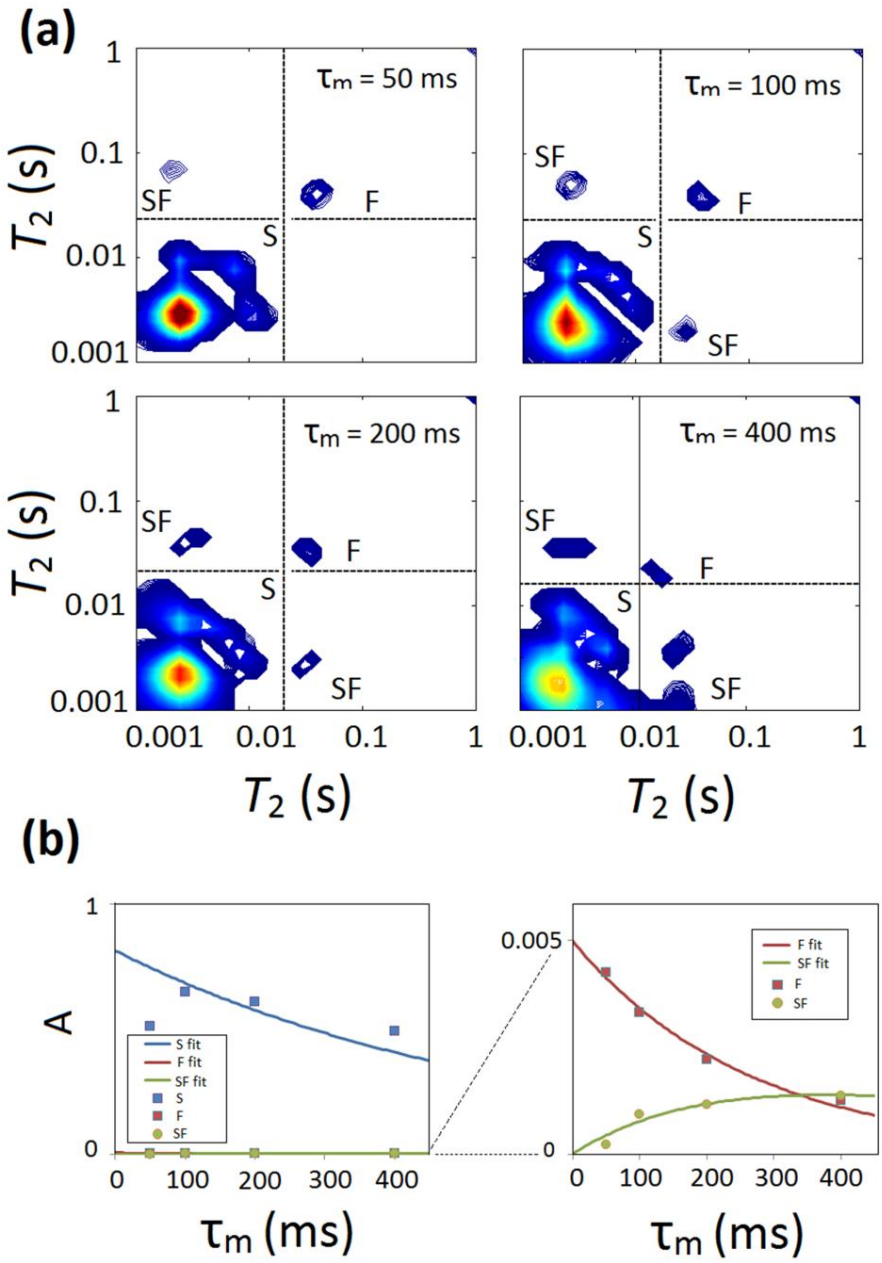

Figure S7. (a) T_2-T_2 relaxation exchange maps for the anion as a function of the mixing time at 296 K. (b) Integrals of the peaks as a function of the mixing time. Fits of the two-site exchange model to the data are shown by solid lines. The resulting exchange rate is k = 1.3±0.3 s^{-1} (k_{SF} = 0.008±0.002 s^{-1}, k_{FS} = 1.3±0.3 s^{-1}).

3. Relaxation data in terms of a microscopic model

In reference [3], diffusion data on the $[P_{6,6,6,14}][BMB]$ system is qualitatively discussed in terms of electrostatic interactions. In particular, two *different* diffusion constants are estimated at room temperature. The detailed relaxation and diffusion experiments provided in this work enable a discussion of low temperature data in terms of a microscopic model that supports a picture with aggregated and individual ions.

3.1 IL relaxation models

It has been shown possible to measure the translational diffusion coefficients in ionic liquids [4] via the inter-molecular dipole-dipole (inter-DD) relaxation mechanism in combination with the low field $1/T_1=R_1$ experiments. In this NMR dispersion (NMRD) technique, *i.e.*, $R_1(\omega)$ versus resonance frequency ($\omega=\gamma_H B_0$, where γ_H is the proton gyromagnetic ratio and B_0 the static magnetic field) slow dynamics is probed that influence the spin relaxation. The T_2 relaxation measured in this work has a dependence on zero frequency spectral density (introduced below) and is thus also expected to have a significant dependence on the slow molecular dynamics.

Several works considered ionic-liquid NMRD relaxation modelled with translational diffusion and intermolecular (inter-DD) as a dominating low-field mechanism [4-7]. However, recently [8] this view on possible relaxation mechanism is contrasted, showing that the NMRD profiles can be rationalised using intra- and inter-ionic spin DD interactions, where anions are mainly modulated by ionic reorientation because of temporary correlations with cations, where the modulation by translational diffusion only plays a minor role. In the system of reference [8] the estimated ion-pair reorientation correlation time is slow at nano-second time scale. An ionic system with a different anion compared to our study ($[P_{6,6,6,14}][Cl]$) was explored with NMR relaxometry [7]. In reference [7] a biexponential $1/T_1$ was observed and the two processes where attributed to the cation-proton spin density of CH_2 and CH_3 respectively.

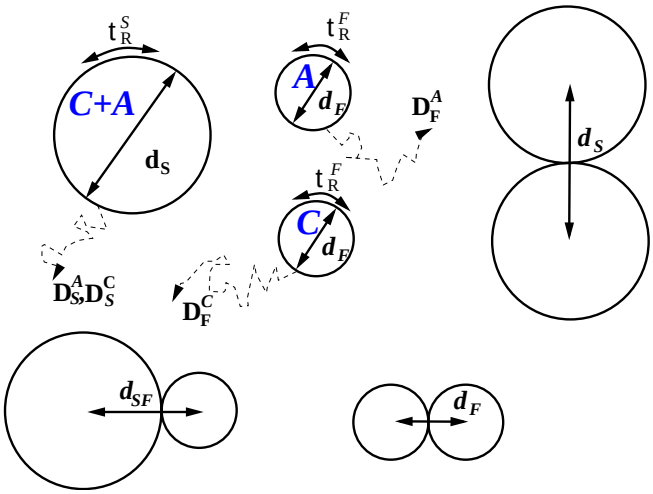

Figure S8. Scheme of a relaxation model, *C*: cation, *A*: anion, *F*: fast diffusing molecule, *S*: slow diffusing *A+C* complex, d_S: closest contact distance for S, d_F: closets contact distance for *A* or *C*, the contact distance for *S-F* is $d_{SF}=1/2(d_S+d_F)$.

In this work LNMR provide detailed experimental information with the *D*-T_2-map (*D* denoting diffusion constant) and T_1 rates. A relaxation model needs in this case to explain both the anion and the cation observations. A hard-sphere relaxation model is considered, assuming a homogenous sample [4, 9], where aggregate or free ions dynamics determine the NMR relaxation mechanisms: intra-DD, intra-CSA (chemical shift anisotropy) and inter-DD. The scheme is depicted in Figure S8, where the experimentally determined diffusion constants are proposed to be an anion-cation complex as the slowly diffusing entity (*S*) and the fast diffusion (*F*) is either observed with cation (*C*) or anion (*A*) spins, the later for simplicity assumed to have equal diameters. Other processes that may contribute to the NMR relaxation can come from the association and breaking of ion complexes, modulating the chemical shift [8]. Such process may be implicitly present in the extreme-narrowing factor denoted "α_x, *x=C,A*" in Eq. S3 below, introduced as a factorised relaxation contribution. Given the experimental observation of *F* to *S* exchange at 1.11 s^{-1} suggests that an association-breaking process is too slow at 296 K in comparison with the observed millisecond T_2, to form a significant field-dependent mechanism. The relaxation rate for slowly diffusing cations (*SC*) is given by:

$$R_{\mathrm{i}}^{SC}(\omega) = R_{\mathrm{i,intra}}^{DDSC}(\omega) + R_{\mathrm{i,intra}}^{CSASC}(\omega) + R_{\mathrm{i,inter}}^{DDSC}(\omega) + \alpha_C, \ (\mathrm{i} = 1,2)$$
$$R_{\mathrm{i,inter}}^{DDSC}(\omega) = R_{\mathrm{i,inter}}^{SCSC}(\omega) + R_{\mathrm{i,inter}}^{SCSA}(\omega) + R_{\mathrm{i,inter}}^{SCFC}(\omega) + R_{\mathrm{i,inter}}^{SCFA}(\omega), \quad \text{(S3)}$$

with the corresponding *FC*, *SA* and *FA* rates given by alternating the superscripts. In Eq. S3 $1/T_1$ and $1/T_2$ have i=1 and i=2 respectively, ω is the proton resonance frequency; the three types of inter-DD contributions for SC are: interaction with the S-complex (SC-SC and SC-SA), the fast diffusing cation (SC-FC) and the fast diffusing anion (SC-FA). The proton chemical shift anisotropy (*CSASC*) is included as well. The experimental data are provided in Table S1, where the explicit rates for *SC*, *DC*, *SA* and *FA* are provided for T_2 and D, whereas for T_1 only the single *C* or *A* observation is recorded. The model for $1/T_1$ rate is a combined weighted contribution:

$$R_1^y(w) = P_s R_1^{sy}(w) + (1 - P_s) R_1^{fy}(w), \quad y = C, A \quad \text{(S4)}$$

where $P_s \in [0,1]$ is the fraction proton spins of slowly diffusing compound. The individual relaxation rate contributions are computed from [4, 10]:

$$\begin{aligned}
R_{\mathbf{1,intra}}^{DDSC}(\omega) &= 2C_{DD}^2\left[J_{\mathbf{intra}}^{S}(\omega) + 4J_{\mathbf{intra}}^{S}(2\omega)\right],\\
R_{\mathbf{2,intra}}^{DDSC}(\omega) &= C_{DD}^2\left[3J_{\mathbf{intra}}^{S}(0) + 5J_{\mathbf{intra}}^{S}(\omega) + 2J_{\mathbf{intra}}^{S}(2\omega)\right],\\
R_{\mathbf{1}}^{CSASC}(\omega) &= (2/15)(\omega\Delta\sigma_{CSA}^{C})^2\left[J_{\mathbf{intra}}^{S}(\omega)\right],\\
R_{\mathbf{2}}^{CSASC}(\omega) &= (1/15)(\omega\Delta\sigma_{CSA}^{C})^2\left[4/3J_{\mathbf{intra}}^{S}(0) + J_{\mathbf{intra}}^{S}(\omega)\right],\\
R_{\mathbf{1,inter}}^{SCFC}(\omega) &= 2K_{DD}^{FC}\left[J_{\mathbf{inter}}^{S,FC}(\omega) + 4J_{\mathbf{inter}}^{S,FC}(2\omega)\right],\\
R_{\mathbf{2,inter}}^{SCFC}(\omega) &= K_{DD}^{FC}\left[J_{\mathbf{inter}}^{S,FC}(0) + 5J_{\mathbf{inter}}^{S,FC}(\omega) + 2J_{\mathbf{inter}}^{S,FC}(2\omega)\right],\\
K_{DD}^{FC} &= \frac{2}{5}I_H(I_H+1)N_{FC}\frac{1}{d_{SF}^3}\left(\frac{\mu_0}{4\pi}\gamma_H^2\hbar\right)^2,\\
C_{DD}^2 &= \frac{1}{5}I_H(I_H+1)\left(\frac{\mu_0\gamma_H^2\hbar}{4\pi r_{eff}^3}\right)^2,
\end{aligned} \quad \text{(S5)}$$

where d_{SF}=1/2(d_S+d_F) (or d_S, d_F) are the close-contact distances (see Figure S8), N_{FC} is the *FC* proton spin density, the spin quantum number is I_H=1/2, $\hbar$ is the Planck constant in angular units, μ_0 is the vacuum permeability and the intra-DD constant (C_{DD}) depends on the effective proton distance r_{eff}. The inter-DD interaction is assuming spins located at the centre of the spheres. The second rank chemical shift anisotropy [10] is given by $\Delta\sigma^{x}_{CSA}$ (for x=*A*,*C*) in parts per million (ppm).

Table S1: Experimental translational diffusion (m^2s^{-1}) and relaxation rates, the later at two magnetic fields.

	D^{SC}=9.6e-14	D^{FC} =3.0e-12	D^{SA}=9.7e-14	D^{FA}=4.0e-12		
Field (T)	T_2^{SC} (ms)	T_2^{FC} (ms)	T_2^{SA} (ms)	T_2^{FA} (ms)	T_1^{C} (s)	T_1^{A} (s)
7.04	6.0	69	4.5	55	0.56	0.56
14.09	5.5	80	4.5	72.5	0.96	0.96

3.2 Model dynamics

Hard sphere intramolecular spectral densities are computed from

$$J^{x}_{\mathbf{intra}}(nw) = \frac{t^{x}_{\mathbf{R}}}{1+(nwt^{x}_{\mathbf{R}})}, \tag{S6}$$

for *x*=*A*,*C* where τ^{x}_{R} is the second rank rigid body rotational diffusion correlation time.

The inter-DD spectral density is given by the hard sphere translational diffusion model [5, 11], in the analytical format (see page 61 in reference 10). The dominating inter-DD zero frequency spectral densities for T_2 are proportional to the characteristic correlation times (depending on self and cross interacting spins respectively, see Figure S8):

$$t_D^{FC} = \frac{d_F^2}{2D_{FC}}; \quad t_D^{FA} = \frac{d_F^2}{2D_{FA}}; \quad t_D^{SC} = t_D^{SA} = t_D^{S} = \frac{d_S^2}{2D_S};$$
$$t_D^{SyFx} = \frac{d_{SF}^2}{D_S + D_{Fx}}; \quad t_D^{FyFx} = \frac{d_F^2}{D_{Fy} + D_{Fx}}, \quad x=(C,A), y=(C,A); \tag{S7}$$

3.3 Model parameters

Inter-DD relaxation depends on the molecule size (here simplified as the diameters of two spheres) and the experimentally known translational diffusion constants, as well as the proton spin densities (NSC, NSA, NFC and NFA). Proton spin densities are computed from the fraction of slow diffusing spins (model parameter *Ps*) and the mass density of the system at 298 K [1]. Note that *Ps* also enter the model in $1/T_1$ calculation (see Eq. S4). The molecular rotational correlation time for molecule Y (Y=*S*,*FC*,*FA*) is $\tau_R^Y = \tau_D^Y \cdot C$ (see Eq. S7), where theoretically *C*=1/9 for the force free diffusion model

obtained by relating the hydrodynamic radius for translational and rotational diffusion [9]. This constant is typically found to be smaller in "real" liquids [9], and is kept as an adjustable parameter in this study. There are a few fast processes that contribute to the extreme narrowing terms (α in Eq. S3) that may include intramolecular carbon chains motion and chemical shift modulation from ion-ion cluster formation [8]. These field independent contributions are not considered explicitly by analysing the difference:

$$\Delta R^{y} = R_2^{y} - R_1^{y}, \quad (y = A, C) \tag{S8}$$

for *S* and *F*, respectively. For the majority of relaxation mechanisms α cancel out [10] (see Eqs. S5 and S8). Caution is needed with the CSA mechanism where $1/3\alpha^{CSA}$ formally remains [10]. However, fast processes have a small influence on the dominating R_2 in Eq. S8; hence, this will at most cause a minor deviation. The explicitly modelled CSA contribution is performed with two fixed CSA constants for the anion and the cation, respectively. The cation have protons bound to CH_2 and CH_3, whereas for the anion double-bond carbons provide the proton sites, hence, the ions can be expected to have different CSA constants. In order to avoid additional adjustable parameters quantum chemistry estimates [12] at 1 ppm and 3.7 ppm are used for *C* and *A*, respectively (assuming zero asymmetry parameter for CSA). The intra-DD coupling C^{DD}, represents a large number of DD interactions, and is kept as an adjustable parameter from which the r^{-6} weighted effective H-H distance (r_{eff}) is extracted.

3.4 Model results

The model results are given in two main sections; the first part presents the experimental and model results for a range of spin-fractions of the slow-diffusion complexes (P_S), analysed with conventional minimization routine. Secondly, the important reliability of the model parameters are analysed using Monte Carlo simulations.

The deviation from experimental ΔR is formulated as a mean-square error (MSE):

$$MSE = \frac{1}{(N - M)} \sum_{i=1}^{N} \frac{\left(\Delta R_i^{EXP} - \Delta R_i^{MODEL}\left[d_S, d_F, C^{DD}, C\right]\right)^2}{2\sigma_i^2}, \tag{S9}$$

with N(=8) ΔR^{EXP} (see Eq. S8), involving eight T_2, and four T_1. Four experimental diffusion constants are fixed parameters in the ΔR^{MODEL}, $(\sigma_i^2)^{-1}$ is the weight of observation "*i*", here set to unity. The

M(=4) fitting parameters are: d_S, d_F, C^{DD} and C, where the last parameter is the fraction of rotational and translational diffusion correlation times. With a MATLAB implementation of *MSE* (Eq. S9) minimisations are done with the Nelder-Mead (Simplex) method [13], providing an unconstrained parameter search. First, a screening with P_S in the range from zero to 100 % in steps of 0.5 % was performed. This revealed a lowest $(MSE)^{1/2}$ for P_S>95 % with minima at spin fractions 99.5 % and 0.5 % for slow and fast diffusing spins, respectively. In Table S2 representative fitting results are shown with the model parameters, $(MSE)^{1/2}$, the spin-fraction (P_S) and model correlation times for *S* and *F* rotational diffusion. A general feature of the screening result is that the minima of $(MSE)^{1/2}$ may be obtained with unphysical model parameters (highlighted in red). For instance, the short 1.3 Å effective H-H distance is shorter than estimated minimal H-H distance at ca. 1.7 Å in CH_2; secondly, rotational- and translational-diffusion correlation time ratios (C) that are larger than 1/9 suggest that rotational diffusion is faster than a force-free motion. To discuss the model further both a restricted parameter search needs to be considered as well as a realistic error estimation of the parameters. These aspects are solved in the next subsection with Monte Carlo simulations.

Table S2: Minimisation result (*MSE*, see Eq. S9) for relaxation rates recorded at two frequencies: 300 and 600 MHz for a range of spin fractions of slowly diffusing complexes (P_S). The fitted parameters are the diameters of slowly and faster diffusing complex/ion (d_S) and (d_F), respectively, the ratio (C) of rotational and translational correlation times and the effective intramolecular proton-proton distance (r_{eff}, extracted from intra-DD). Diffusion constants (included as fixed parameters in the model) and measured relaxation rates are listed in Table S1, a total of 16 experimental observations. CSA parameters from section 2.3 are used. A general feature of the screening result is that the minima of $(MSE)^{1/2}$ may be obtained with unphysical model parameters (highlighted in red).

Fitted parameters							
d_S (Å)	d_F (Å)	C	r_{eff} (Å)	$(MSE)^{1/2}$	P_S (%)	τ_R^{SC} (μs)	τ_R^{FC} (ns)
12	6.3	**1.0**	5.0	10.6	100	7.1	66
87	21	1.8e-2	5.0	10.5	99.5	7.0	10
12	6.9	**0.9**	5.0	10.5	99	7.0	54
4.5	4.1	**6.4**	7.2	10.6	98	7.0	140
4.9	4.5	**5.6**	6.4	10.6	97	7.0	140
30	13	**4.6**	5.9	10.7	96	7.0	150
32	14	6.9e-2	4.2	13.4	95	3.7	16
7.5	8.1	**2.4**	5.2	10.9	90	7.0	200
573	611	4e-4	4.6	11.8	50	7.2	200
25	29	1.7e-3	4.6	10.8	10	7.0	390
37	51	5.8e-5	**1.3**	17.8	2	4e-3	0.2
2.4e+4	**3.6e+4**	2.9e-4	4.6	10.7	1	7.0	380

3.5 Parameter error estimation

The best-fit spin fraction case (P_S=99.5 % in Table S2) is explored further in this section. This is done by considering the maximum likelihood of the $MSE^{1/2}$ (see Eq. S9), hence, where $MSE^{1/2}$ have a Gaussian probability distribution and implement Markov-chain Monte Carlo [14] (MCMC) to sample the unknown four-dimensional parameter distribution. This enables realistic estimation of parameter error bounds for a given set of constraints. The MCMC sampling was done following the Metropolis-Hastings algorithm [14] where initial configurations are generated uniformly and kept within the constraints (see Table S3) by implementing reflective boundary condition. After simulating an initial "burn in" period the productive estimation [14] follows. Four trajectories with 1e+7 MCMC-steps where generated. Given these trajectories it is seen that the target distribution

does not depend on the initial condition [14]. In Figure S9 the normalised projected 1D histograms are given. First we note that the range of the histograms in Figs. S9a-S9c does not reach the boundaries in Table S3 for the parameters d_F, d_S and C^{DD}. However, for the ratio $C=\tau_R/\tau_D$ (Fig. S9d), the MCMC reaches the boundaries at 0.005 and 0.111, respectively. These boundaries are chosen with the force free diffusion as the maximum and the minimum are set to smaller values than typically found for normal liquids and ionic liquids [4, 15]. Note that larger C than the force free diffusion, the 1/9 introduced above in section 3.3, points towards an inconsistent model since these ion clusters are expected to entangle and interact significantly. From the MCMC trajectories parameters are estimated with the mean values (d_F=20.5 Å, d_S=82 Å, r_{eff}=4.68 Å and C=0.035) and a 95 % probability error interval from the integration of the histograms providing 15<d_F<31 Å, 50<d_S<160 Å, 4.62<r_{eff}<4.75 Å and 0.01<C<0.1. Hence, the S sphere is distinctly larger than the F sphere. Other properties of interest are straightforward to estimate, such as the ratio of the S and F model volumes $V_S/(2V_F)$ that has a mean of 32 with 95 % probability interval 10<$V_S/(2V_F)$<66. Hence, if the fast diffusing entity are individual ions and the complex is neutral, the model predicts the complex to contain more than 10 and less than 66 ion-pairs with 95 % probability.

Finally, it is interesting to explore the role of CSA. In Figure S10 bar plots of the $1/T_2$ rates without and with the CSA relaxation mechanism in Figs. S10a and S10b, respectively (models are optimised at P_S=99.5 % following Section 3.4 with the resonance frequency of protons 600 MHz). However, note that the optimisation is done for the difference presented in Eq. S8. Although the $MSE^{1/2}$ is factor 1.7 smaller including the CSA contribution, the physical picture is the same, showing a slowly diffusing complex, where $1/T_2$ is dominated by the intra-DD and for fast diffusing ions the mechanism is inter-DD. Also without CSA the slowly diffusing complex is of a larger dimension (d_S>d_F). However, the CSA should not be ignored on physical grounds at these high magnetic fields and, in addition, improves the analysis by reducing the MSE. In this work the extreme narrowing contributions (see α in Eq. S3) are not explicitly modelled and thus $1/T_1$ is underestimated in a direct comparison. In particular, the diffusion modulated intermolecular $1/T_1$ contribution is negligible.

3.6 Summary

It is found that a microscopic relaxation model is consistent with the picture of large aggregates (mean diameter of 82 Å) undergoing slow translational diffusion and with rotational correlation time

7 µs, containing 99.5 % of the proton spins; complemented with smaller entities (mean diameter of ca. 20 Å) rotating with correlation time of 10 ns. Markov-chain Monte Carlo simulation with the proposed model provides consistent results with the conventional minimisation and is essential in order to conclude on the reliability of the suggested model.

Table S3: Parameter boundaries in the MCMC simulation.

Boundary	d_F (Å)	d_S (Å)	C^{DD} (s^{-1})	C
Min	2	5	0.75	0.005
Max	1000	2000	7.54e+5	0.111

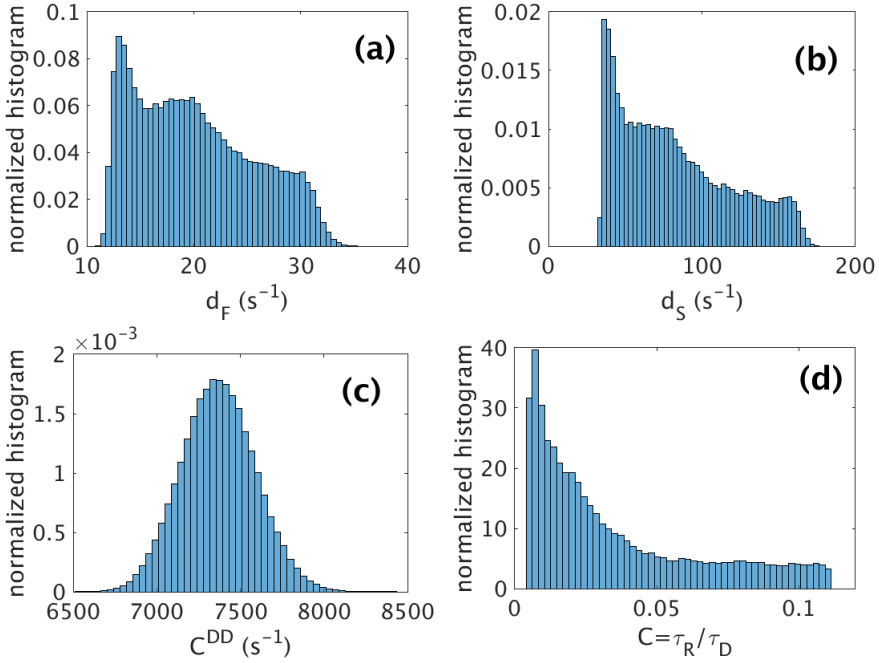

Figure S9. Histogram from MCMC simulation (with P_S=99.5 %) for parameters d_F (**a**), d_S (**b**), C^{DD} (**c**) and C (**d**).

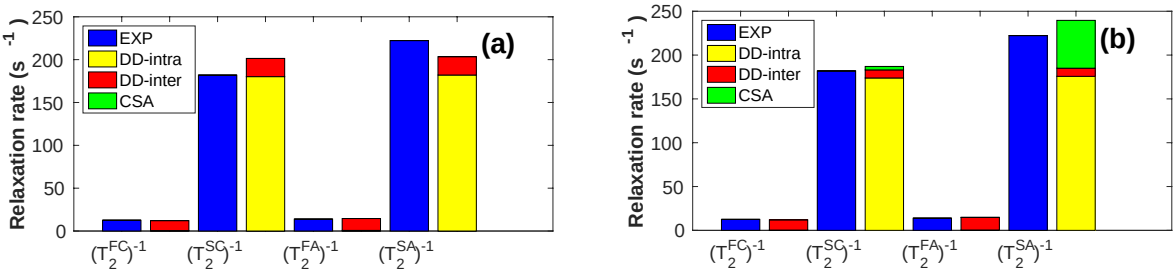

Figure S10. Experimental and computed $1/T_2$ rates excluding (**a**) and including (**b**) the CSA relaxation mechanism. Proton resonance frequency is 600 MHz and the computed rates are for parameters optimised at P_S=99.5 %.

4. References

[1] F. U. Shah, S. Glavatskih, D.R. MacFarlane, A. Somers, M. Forsyth, O.N. Antzutkin, *Phys. Chem. Chem. Phys.,* **2011**, 13, 12865-12873.

[2] J. A. Aguilar, M. Nilsson, G. Bodenhausen, G. A. Morris, *Chem. Commun.,* 2012, **48**, 811-813.

[3] A. Filippov, F. U. Shah, M. Taher, S. Glavatskih, O. N. Antzutkin, *Phys. Chem. Chem. Phys.*, **2013**, 15, 9281-9287.

[4] D. Kruk, R. Meier, A. Rachocki, A. Korpała, R. K. Singh, E. A. Rössler, *J. Chem. Phys.*, **2014**, 140, 244509.

[5] Y. Ayant, E. Belorizky, J. Alizon, J. Gallice, *Le J. Phys.*, **1975**, 36, 991-1004.

[6] Y. Ayant, E. Belorizky, P. Fries, J. Rossiet, *Le J. Phys.*, **1977**, 38, 325-337.

[7] C. I. Daniel, F. V Chavez, C. A. M. Portugal, J. G. Crespo, P. J. Sebastião, *J. Phys. Chem. B*, **2015**, 119, 11740-11747.

[8] P.-O. Westlund, G. Driver, Y. Wang, T. Sparrman, A. Laaksonen, Y. Huang, *Phys. Chem. Chem. Phys.*, **2017**, 19, 4975-4988

[9] D. Kruk, R. Meier, E. A. Rössler, *J. Phys. Chem. B*, **2011**, 115, 951-957.

[10] J. Kowalewski and L. Mäler, *Nuclear Spin Relaxation in Liquids: Theory, Experiments, and Applications*, Taylor & Francis Group, New York, U.S.A., **2006**.

[11] L.-P. Hwang, J. H. Freed, *J. Chem. Phys.*, **1975**, 63, 4017-4025.

[12] J. Kaski, P. Lantto, J. Vaara, J. Jokisaari, *J. Am. Chem. Soc.*, **1998**, 120, 3993-4005.

[13] W. H. Press, S. A. Teukolsky, W. T. Vetterling, B. P. Flannery, *Numerical Recipes in C: The Art of Scientific Computing*, Cambridge University Press, New York, 2nd Ed., **1992**.

[14] U. von Toussaint, *Rev. Mod. Phys.*, **2011**, 83, 943-999.

[15] R. Meier, R. Kahlau, D. Kruk, E. A. Rössler, *J. Phys. Chem. A*, **2010**, 114, 7847-7855.